Sensors & Actuators: B. Chemical 423 (2025) 136863

Contents lists available at ScienceDirect

Sensors and Actuators: B. Chemical

journal homepage: www.elsevier.com/locate/snb

Straightforward electroanalytical sensing of nitrate in cyanobacteria growth media at electrified liquid-liquid interface

Muthaiah Annalakshmi [a,*], Thangaraj S.T. Balamurugan [a], Karolina Czarny-Krzymińska [b], Karolina Marciniak [a], Lukasz Poltorak [a,*]

[a] Department of Inorganic and Analytical Chemistry, Faculty of Chemistry, University of Lodz, Tamka 12, Lodz 91-403, Poland
[b] Laboratory of Environmental Threats, Department of Inorganic and Analytical Chemistry, Faculty of Chemistry, University of Lodz, Tamka 12, Lodz 91-403, Poland

ARTICLE INFO

Keywords:
Nitrate pollution
Eutrophication
Harmful algal blooms
Ion transfer voltammetry
Microcystis aeruginosa

ABSTRACT

Nitrate is one among the necessary substance in the biosphere as its presence is pivotal to ensuring healthy vegetation and human health while its excess causes serious adversities. In this work, we utilized the electrified liquid-liquid interface (eLLI) and voltammetry to develop an alternative approach that enables onsite periodic monitoring of nitrate ions in cyanobacteria growth medium. The signal attributed to nitrate detection was directly related to its interfacial ion transfer behavior and not the redox properties. The ion transfer voltammograms of nitrate at eLLI delivered useful analytical parameters of linear detection range from 20 to 500 μM paired with detection and quantification limits of 1.5 and 14.6 μM, respectively. Further, the influence of chloride ions, and other anionic species present in the algae grow media were studied towards the determination of nitrates. We also optimized an *in-situ* chemical precipitation strategy to eliminate the influence of chloride ions that significantly improved the accuracy of the eLLI-based nitrate sensor. eLLI-based nitrate sensor delivered a remarkable analytical performance to determine nitrate levels in Z8 medium composed of nitrate and other nutrients (medium serving as the optimal environment for algae growth). eLLI based nitrate sensor was successful towards periodic monitoring of nitrate levels in *Microcystis aeruginosa* cyanobacteria samples cultured in Z8 medium.

1. Introduction

Nitrate is one of the key nitrogen species originating from the natural nitrogen cycle. It is profound in various ecosystems. The role of nitrate in the biosphere is pivotal, especially in plant physiology, and essential for plant growth and development. An optimal amount of nitrate in waterbodies boosts vegetation to ensure the sustainability of aquatic ecosystems [1–3]. In humans, nitrates are supplied through dietary intake of green leafy vegetables, fruits, and drinking water and play a crucial role in the nitric oxide cycle, regulating blood pressure, blood flow, etc., [4,5]. On the other hand, manmade anthropogenic activities have led to elevated levels of nitrates in ecosystems. This in turn triggers serious health risks and environmental hazards [6–8]. In particular, the extensive use of synthetic nitrogen fertilizers is the primary cause of elevated nitrate levels in food, soil, and aquatic systems. The excessive nitrates from agricultural fields ran off into nearby water bodies and led to contamination of surface and groundwater [8,9]. This prolonged aggregation of nitrates in aquatic systems catalyzes rapid growth of algae (harmful algae blooms) and other aquatic plants in much larger quantities (eutrophication) to an extent that blemishes the aquatic system making them inconsumable and inhabitable for other species[10,11]. In humans, the excessive intake of nitrate can trigger carcinogenesis in the gastrointestinal system, liver, and kidneys in adults and blue-baby syndrome in infants [12,13]. In this respect, global health and environmental agencies including the World Health Organization (WHO) and the European Union Directives (EUD) have defined the maximum permissible levels of nitrates at 50 $mg.L^{-1}$ in food and drinking water. Meanwhile, the United States Environmental Protection Agency (USEPA) and the Italian regulations recommend the limits of ~45 $mg.L^{-1}$ for adults and 10 $mg.L^{-1}$ for infants in Italy. In parallel, the EUD, Environmental Protection Agency (EPA), has defined the maximum permissible levels of nitrate in food products as <500 $mg.kg^{-1}$ [13,14]. Thus, developing analytical tools for onsite periodic monitoring of nitrate from various sources is of great research significance with respect

* Corresponding authors.
E-mail addresses: annalakshmi.muthaiah@chemia.uni.lodz.pl (M. Annalakshmi), lukasz.poltorak@chemia.uni.lodz.pl (L. Poltorak).

https://doi.org/10.1016/j.snb.2024.136863
Received 26 July 2024; Received in revised form 20 October 2024; Accepted 27 October 2024
Available online 28 October 2024

to health, environment, and economy [15].

A range of analytical tools have been proposed for the detection of nitrates such as spectrophotometry based technics [16], colorimetric assays [17,18], ion chromatography[19,20], electrophoresis[21,22], electrochemical sensors[6–8], or field effect transistors[23,24], etc., Most of these analytical platforms are laborious, require intensive sampling and testing protocols that necessitates an expert technician to perform the tests and analyze the results. On the other hand, electrochemical sensors stand tall over other technologies all thanks to their minimal sampling, rapid test time, simple analytical procedures, high portability, and low cost to enable on-site testing of nitrates [7–9]. The analytical performance of electrochemical sensors is still far beyond what chromatographic tools can offer, but at the same time these solutions are superior to results offered by the colorimetric techniques and meet the standards for early and on the spot analysis [8]. In particular, nanomaterials-enabled carbon electrodes show great potential for electrochemical detection of nitrates in various sample matrices. The nanomaterials modification aims at (i) minimizing the redox potentials, (ii) triggering high electrocatalytic currents, (iii) limiting surface passivation and electrode fouling to finally (iv) summing up all these features to extend the analytical parameters of the sensors over most commonly utilized bare carbon electrode counterparts[6,7,15]. The necessity to detect and monitor nitrates, nitrites, and other nitrogen-containing species in various environments drives the development of new alternative electroanalytical tools.

Especially, ion-selective electrodes are one such alternative state-of-the-art electroanalytical tool proposed for the detection of various ionic species and so nitrates. The nitrate selective electrodes possess significant advancements in terms of improved analytical parameters and selectivity over the conventional electrocatalytic sensors [25–27]. However, the fabrication of ion-selective membranes is a relatively complex process and usually suffers interference from chloride and chlorate ions[27,28]. Also, ion-selective electrodes usually allow the potential drop monitoring that is ideally attributed to the target analyte ion transfer process, meaning that other possibly happening reactions are discriminated and not being followed. This accelerates the development of alternative electroanalytical tools with new approaches.

Electrified liquid–liquid interface (eLLI) or the interface between two immiscible electrolyte solutions (ITIES) is one such alternative electroanalytical solution that was proven successful in the electroanalytical detections of various biomolecules, drugs, illicit substances, and metabolites [29–32]. Unlike the conventional electrochemical sensors where the analytical signals originate from the redox reaction (either direct or indirect) happening at the surface (or in its proximity) of the solid electrode, the analytical signals at eLLI are due to the ion transfer between two mutually immiscible electrolyte solutions. This interfacial ion transfer is enabled by the difference in Galvani potential at the liquid junction. The ion transfer reactions and analytical parameters are governed by molecular partitioning properties of the target analyte (existing in either phase) compromised especially when co-existing species (in the investigated matrix) undergo ion transfer reactions within polarizable potential window[29,32]. The difference in partitioning properties (formal Galvani potential difference of the studied ions) between the target analytes and coexisting species enables selective detection of analytes of interest from complex sample environments.

Our team has been successful in developing eLLI-based electroanalytical solutions for the rapid screening of drugs, biomolecules, and significant metabolites in complex sample media [33–37]. In addition, eLLI can also be employed to study the interfacial properties of various molecules including proteins, macromolecules, molecular associates, etc., for analytical, physiological, and physiochemical purposes[38,39]. Although the aspect of nitrate detection at the eLLI seems to be an intuitive option, there is a lack of information on how and under which circumstances soft junction can be used for this target analyte quantification. A report of nitrate ions behavior at eLLI was reported by Tom *et al.*, who aimed at study the interfacial characteristics of alkylphosphonium ionic liquids and does not study the analytical attributes of nitrate and eLLI [40]. Another example published by Qian *et al.* allows for nitrate detection derived from the anion transfer reaction facilitated by N-{2-[Bis[2-(4-tert-butylbenzoyl)aminoethyl]amino] ethyl}4-tert-butylbenzamide. The indicated report can be considered as seminal and allowed for nitrate detection with the LOD equal to 0.2 mM (still leaving a place for improvement) [41]. A group of Chen used an anion exchange membrane as the support of the eLLI and showed that different inorganic anions (including nitrate) interfacial transfer can be followed with voltammetry. Interestingly, differential pulse voltammetry could be used to separate signals originating from Cl^-, ClO_4^-, NO_2^- and SO_4^{2-} leaving NO_3^- aside [42].

In this work, we aimed to employ the eLLI as an alternative electroanalytical platform for the periodical monitoring of nitrate levels in cyanobacteria culture medium (Z8 medium)[43]. The key barrier in the periodical monitoring of nitrates in nutrient medium involves the presence of large amounts of other co-existing ionic species (plant nutrients) and chloride ions, in particular (abundant element present in the vast majority of water-based samples). In this respect, we have performed a detailed study on the interfacial behavior of nitrates at eLLI (which to our surprise was missing) formulated between water and 1, 2-dichloroethane solutions to examine the effect of cyanobacteria grow media constituents interference (especially Cl^-) and protocols to minimize their effect. In sequence, a detailed electrochemical profile of plant nutrients composing algae growth medium also has been established. Finally, the developed eLLI system was successfully applied to the periodical monitoring of in-vitro analysis of nitrate levels in *Microcystis aeruginosa* LEGE 91094 cyanobacteria samples with good consistency. A schematic illustration of nitrate sensing at eLLI in a cyanobacteria growth medium is shown in Scheme 1.

2. Experimental section

2.1. Reagents and instruments

All chemicals were of analytical grade and used as received. *Aqueous phase involved utilization of following reagents:* sodium chloride (NaCl, ≥99 %, analytical grade, POCh), sodium sulfate (Na_2SO_4, ≥99 %, Merck), sodium nitrate ($NaNO_3$, ≥99 %, Merck), silver nitrate ($AgNO_3$, ≥99 %, Merck), tetramethylammonium chloride (TMACl, >98 %, Acros Organics). All aqueous solutions were prepared by using demineralized water (Hydrolab®) with a conductivity of < 0.06 $\mu S.cm^{-1}$ at room temperature. The pH of the supporting aqueous electrolytes of NaCl (10 mM and 0.5 mM) and Na_2SO_4 (5 mM) were set to 5.6 and 6, respectively, with a pH meter (Orion STAR, A111, The Netherlands) with a polymer pH electrode (Polilyte Lab, Hamilton, Switzerland).

Organic phase involved the utilization of the following chemicals: potassium tetrakis(4-chlorophenyl) borate (KTPBCl, >98 %, Merck), bis (triphenylphosphoranylidene)ammonium chloride (BTPPACl, 97 %, Merck), and 1,2 dichloroethane (1,2-DCE, 99 %, ReagentPlus, Merck). Additionally, an organic electrolyte salt of bis(triphenylphosphoranylidene)ammonium tetrakis(4-chlorophenyl) borate (BTPPATPBCl) was prepared by using the above two chemicals, this is an equimolar mixture of KTPBCl and BTPPACl.

Algae nutrients: calcium nitrate tetrahydrate ($Ca(NO_3)_2.4H_2O$, 99 %), magnesium sulfate heptahydrate ($MgSO_4.7H_2O$, >98 %), dipotassium hydrogen phosphate (K_2HPO_4, ≥98 %), sodium carbonate (Na_2CO_3, ≥99.5 %), iron(III) chloride hexahydrate ($FeCl_3.6H_2O$, 97 %), hydrochloric acid (HCl, for analysis, 37–38 %, ChemPure), ethylenediaminetetraacetic Acid (EDTA, ≥98.5 %), sodium hydroxide (NaOH, ≥99 %, for analysis, POCh), sodium tungstate dihydrate ($Na_2WO_4.2H_2O$, ≥99 %), ammonium molybdate dihydrate ($(NH_4)_6Mo_7O_{24}.2H_2O$), potassium bromide (KBr, >99 %), potassium iodide (KI, >99 %), zinc sulfate heptahydrate ($ZnSO_4.7H_2O$, 99 %), cadmium nitrate tetrahydrate ($Cd(NO_3).4H_2O$, 98 %), cobalt(II) nitrate hexahydrate ($Co(NO_3)_2.6H_2O$, 98 %), copper(II) sulfate pentahydrate

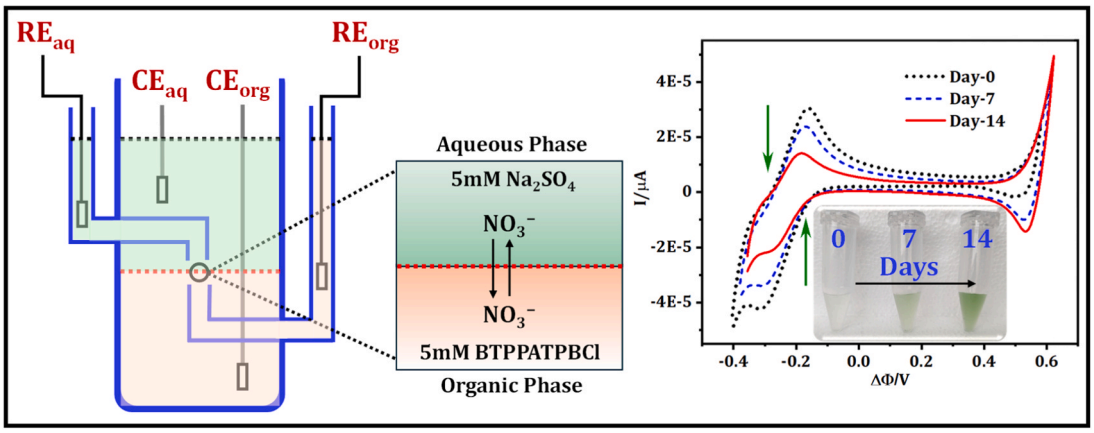

Scheme 1. Pictographic model of periodic determination of nitrate at eLLI in cyanobacteria growth samples.

($CuSO_4.5H_2O$, >98 %), ammonium nickel (II) sulfate hexahydrate ($NiSO_4(NH_4)_2SO_4.6H_2O$, ≥98 %), chromium nitrate nanohydrate ($Cr(NO_3)_3.9H_2O$, 99 %), vanadium (V) oxide (V_2O_5, <98 %), aluminum potassium sulfate dodecahydrate ($AlK(SO_4)_2.12H_2O$, ≥98 %), boric acid (H_3BO_3, ≥99.5 %), manganese sulfate tetrahydrate ($MnSo_4.4H_2O$, 98 %). All these chemicals were purchased from Merck.

2.2. Electrochemical experiments

All electrochemical experiments were performed with either Autolab-PGSTAT 128 N or Autolab-PGSTAT204 potentiostat-galvanostat connected with NOVA 2.1 software (Metrohm Autolab B.V., Netherlands) in a four-electrode configuration. The Ag/Ag_2SO_4 and Ag/AgCl wires were used as reference electrodes for the aqueous and the organic phase, respectively (this was dependent on the aqueous phase composition). While platinum (Pt) wires served as the counter electrodes for both the aqueous and the organic phases. Whenever the x-axis of the shown voltammograms is given as the Galvani potential difference scale the calibration was done based on the tetramethyl ammonium chloride (TMA^+Cl^-) formal Galvani potential difference equal to 0.16 V [34]. The eLLI are formulated in a cylindrical glass electrochemical cell with an inner diameter and height of 1.35 × 5.46 cm paired with two Lugging capillaries placed at a fixed distance of 5 mm. The standard volumes for aqueous and organic electrolytes are kept to be 2.5 and 3.5 mL respectively. On top, the Lugging capillaries of the organic phase are loaded with 0.1 mL of reference electrolyte. Upon examining algal growth samples in Z8 medium the aqueous phase is spiked with fixed quantities (15.5 – 93 μL) of *Microcystis aeruginosa* samples in Z8 medium without any presampling.

The eLLI is formulated with two (aqueous and organic) different electrolyte solutions. The organic phase is formulated with a fixed supporting electrolyte of highly lipophilic 5 mM BTPPATPBCl in 1,2 DCE. The aqueous phase of eLLI is custom-made to meet specific experimental conditions defined from Cell-I to Cell-VI. A typical representation of electrochemical cells used for the detection of nitrates is shown below.

Cell-I: (aq) Ag/AgCl | 10 mM NaCl + *x* μM $NaNO_3$ || 5 mM BTTPPATPBCl |10 mM BTPPACl +10 mM NaCl | Ag/AgCl (org)

Cell-II: (aq) Ag/AgCl | 0.5 mM NaCl + *x* μM $NaNO_3$ || 5 mM BTTPPATPBCl | 10 mM BTPPACl +10 mM NaCl | Ag/AgCl (org)

Cell-III: (aq) Ag/Ag_2SO_4 | 5 mM Na_2SO_4 + *x* μM $NaNO_3$ || 5 mM BTTPPATPBCl | 10 mM BTPPACl +10 mM NaCl | Ag/AgCl (org)

Cell-IV: (aq) Ag/AgCl | 0.5 mM NaCl + *x* μM $AgNO_3$ || 5 mM BTTPPATPBCl | 10 mM BTPPACl +10 mM NaCl | Ag/AgCl (org)

Cell-V: (aq) Ag/Ag_2SO_4 | 5 mM Na_2SO_4 + *x* μM $AgNO_3$ || 5 mM BTTPPATPBCl | 10 mM BTPPACl +10 mM NaCl | Ag/AgCl (org)

Cell-VI: (aq) Ag/Ag_2SO_4 | 5 mM Na_2SO_4 + *x* μM algae nutrient solutions (or) *x* μM algae samples || 5 mM BTTPPATPBCl | 10 mM BTPPACl +10 mM NaCl | Ag/AgCl (org)

2.3. Algae cultivation

Microcystis aeruginosa LEGE 91094 strains were obtained from Blue Biotechnology and Ecotoxicology Culture Collection (LEGE-CC). Cyanobacteria cultures were cultivated in a phytotron chamber (Pol-Eko) under the following conditions: 19°C at a light intensity of 30 μmol photons $m^{-2}.s^{-1}$ and a constant humidity of 30 %, with a light/dark cycle of 12/12 h. Cyanobacteria were cultured in 250 mL Erlenmeyer flask in 100 mL of Z8 medium [44]. The cell densities during the experiment were calculated using a Fuchs-Rosenthal hemocytometer, with an Olympus CX-41 microscope(Olympus).

3. Results and discussion

3.1. Electrochemical characterization of nitrate at eLLI

To start, cyclic voltammograms (CVs) recorded at eLLI formulated with 10 mM $NaCl_{(aq)}$ and 5 mM of $BTTPPATPBCl_{(DCE)}$ (Cell-I) were studied at the potential window of 0.08 – 0.88 V. The CVs display standard ion transfer peaks corresponding to the transfer of chloride ions from the organic to aqueous phase at 0.18 V and the reverse transfer (from the aqueous to the organic phase) observed at <0.2 V. Similarly, the transfer of sodium ions from the aqueous to the organic phase occurs at applied potential higher than 0.80 V [34,45]. Up next, the interfacial behavior of nitrate species in Cell-I were studied with increasing concentration from 0.2 to 1 mM as presented in Fig. 1 A. The CVs display increasing ion transfer currents with increasing concentrations of nitrates within the less positive side of the potential window. Also, we have observed a marginal shift in positive signal from around 0.16 to 0.20 V. This is typical behavior of the eLLI-based systems originating from the organic phase's resistivity that was not compensated during our experiments. A calibration plot of the response current against the concentration of nitrate added to the aqueous phase was found to be linear with a sensitivity of 0.034 $A.M^{-1}$ (Fig. 1B). Even though, the CVs lead to a sequential increase in ion transfer currents with increasing concentration of nitrates, one can notice a significant overlapping between the ion transfer peaks originated from nitrate and chloride ions (see Fig. 1 A). These observations demonstrate potential interference of chloride ions towards nitrate detection in the composed Cell-I system. In this respect, the composition of the aqueous phase was switched from 10 mM to 0.5 mM NaCl as indicated in Cell-II. The CVs of the newly composed Cell-II and interfacial activity of nitrate ion transfers were recorded and are shown in Fig. 1 C. The ion transfer voltammograms (ITVs) of Cell-II with increasing concentrations of nitrate (0.2–1 mM)

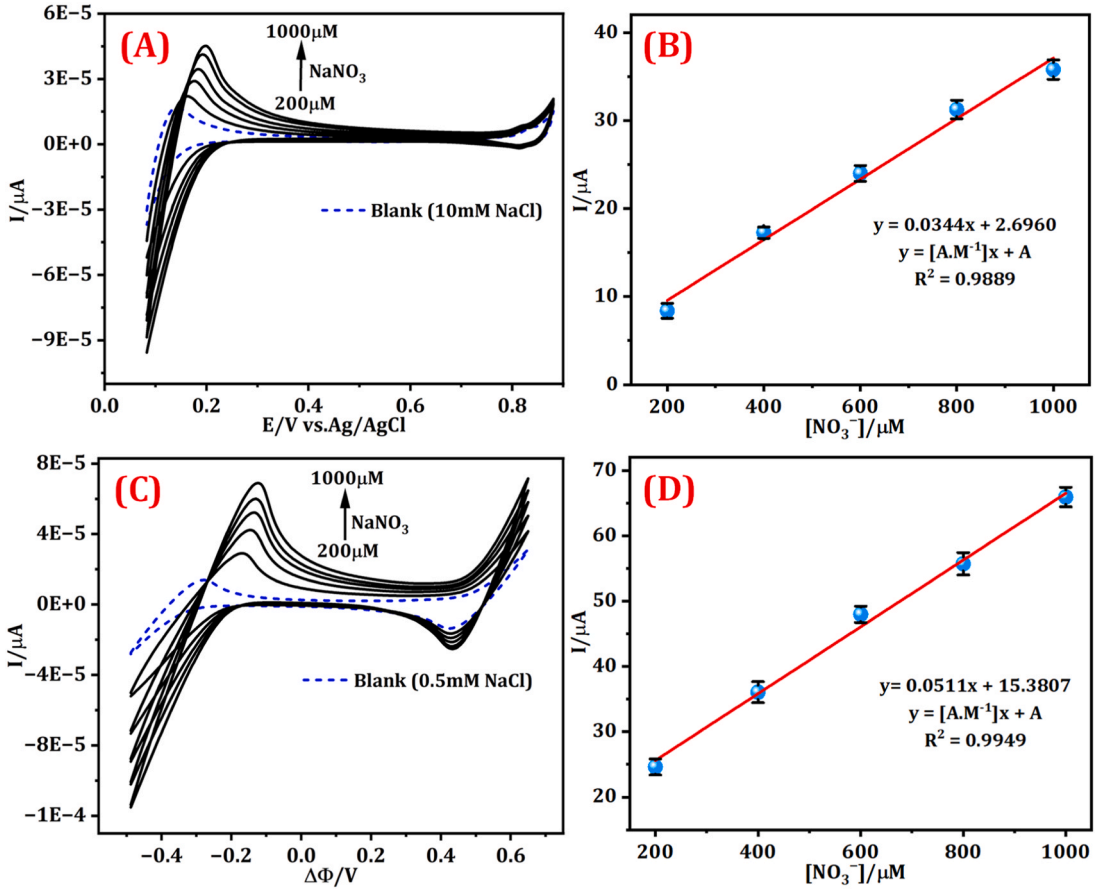

Fig. 1. (A) CVs of $NaNO_3$ recorded in Cell-I, (B) Linear plot between response current (positive peak at around 0.2 V) and concentration of $NaNO_3$ in Cell-I, (C) CVs of $NaNO_3$ recorded for Cell-II, (D) Linear plot between peak current (Galvani potential difference of around −0.10 V) and concentration of $NaNO_3$ in Cell-II.

displayed a broad ion transfer peak with a sequential shift towards higher ion transfer potentials. A plot of nitrate concentration against response current displayed a linear relationship with an improved sensitivity of 0.051 $A.M^{-1}$ (Fig. 1D). This study illustrates that the ion transfer currents of nitrate improved with the drop of chloride concentrations (i.e. the chloride ions have to be eliminated to improve the analytical resolution of nitrate ion transfer) at the eLLI system. Also, it is clear that the effect of chloride ions on the nitrate ion transfer should be studied in detail to fully understand this system limitations.

3.1.1. *Nitrate ion transfer in the absence of Cl^-*

In sequence, the impact of chloride ions present in the aqueous phase part of the eLLI on the nitrate ions interfacial transfer was evaluated in two types of electrochemical cells having a composition as described in Cell-II and Cell-III. The aqueous phase of Cell-III is made of 5 mM Na_2SO_4 replacing the NaCl (chloride ion source) used as electrolyte. The CVs recorded in Cell-II and Cell-III were recorded with and without nitrate ions in the presence of tetramethyl ammonium chloride model ion (TMA^+Cl^-) (red lines in Fig. 2; signal originating from the TMA^+ served as the internal calibration standard and the reference point for the nitrate interfacial transfer).

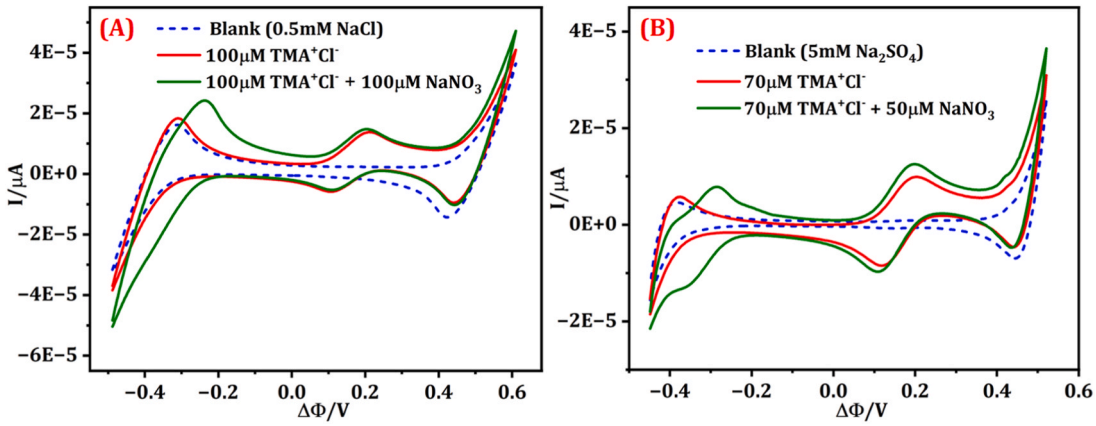

Fig. 2. (A) CV response of 100 μM TMA^+Cl^- in the presence and absence of 100 μM $NaNO_3$ recorded in Cell-II, (B) CV response of 70 μM TMA^+Cl^- in the presence and absence of 50 μM $NaNO_3$ in Cell-III. The scan rate was set to 20 $mV.s^{-1}$.

The CVs recorded in Cell-III (in Fig. 2 A, in the presence of 0.5 mM NaCl) display their characteristic broad ion transfer peak at standard Galvani potential difference of −0.24 V corresponding to nitrate ion transfer, with significant overlap with chloride ion transfer currents. On the other hand, the CV of Cell-III showcased two visible signals towards the transfer of sulfate and nitrate ions at −0.38 and −0.29 V, respectively, (see Fig. 2B). The difference of around 0.11 V (between positive peak potentials recorded for both anions) is sufficient to differentiate between these two chemical species. On the reverse scan, the electrochemical response of Cell-II (Fig. 2 A) showed a significant rise in response current corresponding to the transfer of nitrate ions from the aqueous to the organic phase. Whereas the same polarization range in the absence of NaCl in Cell-III displayed a distinct peak-like signal located at −0.35 V denoting improved signal resolution between sulfate and nitrate ion transfer reactions. These observations have highlighted that Cell-III composed of a sodium sulfate solution aqueous phase (free of chloride ions) offers better signal resolution and can be employed for the detection of nitrate ions at the polarized liquid-liquid interface.

3.2. Electroanalytical detection of nitrate at eLLI

The earlier studies unveil the usability of Cell-III to develop an alternative electroanalytical platform for nitrate determination. The analytical parameters related to nitrate determination in Cell-III (such as detection range, limits of detection, quantification, and sensitivity) were established through a simple CV-based electroanalytical protocol (see Fig. 3). To this, the CVs from Fig. 3 A attributed to Cell-III were recorded in the absence and presence of increasing concentration of $NaNO_3$. As expected, it was found that the increasing concentration of the target analyte (NO_3^-) from 20 to 500 μM resulted in the progressively increasing positive and negative peak current values attributed to the NO_3^- transfer from the organic to the aqueous phase and from the aqueous to the organic phase, respectively. A clear peak-like signal can be observed for both anion transfer directions up to around 200 μM. Since the peak-to-peak separation is increasing along with NO_3^- concentration in the aqueous phase, at some point, the quantification of the negative signal may become a problem as it starts to be overlaid with the background anion transfer (SO_4^{2-} heading from the organic to the aqueous phase) – see Fig. 3 A. The analysis of CVs from Fig. 3 A gave a calibration curves that are shown in Fig. 3B. The wide linear dynamic range 20–500 μM with the linear regression coefficient (R^2) of 0.992 – 0.994 was obtained. Further, the voltammetric sensitivities defined as the slopes of calibration curves, were estimated to be 0.107 and 0.200 $A.M^{-1}$ for positive and negative peak currents, respectively. Furthermore, the limits of detection (LOD) and quantification (LOQ) of the eLLI-based nitrate sensor were calculated to be 1.5, and 14.6 μM, correspondingly. The obtained analytical parameters are on par with that of other existing electroanalytical solutions proposed for the rapid detection of nitrate ions [15,17]. A comprehensive discussion of the analytical parameters of the developed eLLI-based electroanalytical system against the recent reports of electrochemical nitrate sensors is tabulated in Table S1.

3.3. Influence of chloride ions on nitrate detection

The electroanalytical performance of nitrate ion selective electrodes is hugely influenced by chloride and chlorate ions[46,47], with the first being abundant in all types of samples (e.g. water from water bodies, food samples, or even drug formulations). This large influence of chloride and chlorate species can be attributed to their size proximity as the ionic radius of the chloride, chlorate, and nitrate anions were reported to be 172, 171, and 179 pm respectively[48]. This proximity in ionic radius leads to similar charge densities and hydrophilic/hydrophobic properties. This in terms explains why chloride and nitrate species undergo ion transfer processes at similar Galani potential differences (see Fig. 1 A). However, owing to the omnipresent nature of chloride, it is essential to eliminate or minimize its influence to enable rapid detection of nitrate ions at the developed eLLI systems. Notably, the chemical precipitation of chloride as AgCl, CuCl, BiOCl, is one of the most renowned processes to eliminate chloride ions from wastewaters [49,50], and hence, this principle was adopted to eliminate the influence of Cl^- ions affecting nitrate detection at eLLI. Consequently, $AgNO_3$ assisted *in situ* chemical precipitation of chloride ions at eLLI was performed and its effect on interfacial charge transfer processes was studied using the aqueous phase composition as marked in Cell-IV. The CV profiles of eLLI composed of 0.5 mM NaCl were recorded in the absence and presence of increasing concentrations (0.1 – 1.0 mM) of $AgNO_3$ precipitant (see Fig. 4 A). The CVs display two ion transfer peak characteristics to the transfer of nitrate anions (~ −0.21 V) and Ag cations (~0.26 V) across the studied concentration range. Interestingly, the CVs displayed two distinct voltammetric patterns pre and post-equivalent concentration points between the chloride anions (present in the aqueous phase electrolyte of the eLLI) and added Ag^+ (as $AgNO_3$). Beyond the equivalent point, the ion transfer peak (at 0.3 V) corresponding to the Ag cations experienced a downshift to 0.17 V (drop in ion transfer potential) with a significant increase in current amplitude (Fig. 4 A). A plot of $AgNO_3$ concentrations against the response currents of Ag^+ also confirms this trend with two slopes for the ion transfer reactions pre (0.04) and post (0.19) equivalent points (Figs. 4B, 4 C). This fourfold growth in the current signals corresponding to the transfer of Ag^+ ions beyond the equivalent point signifies the occurrence of *in-situ* precipitation of AgCl until the point of ionic equivalence. To testify the hypothesis, the studies are replicated in a medium with no chloride

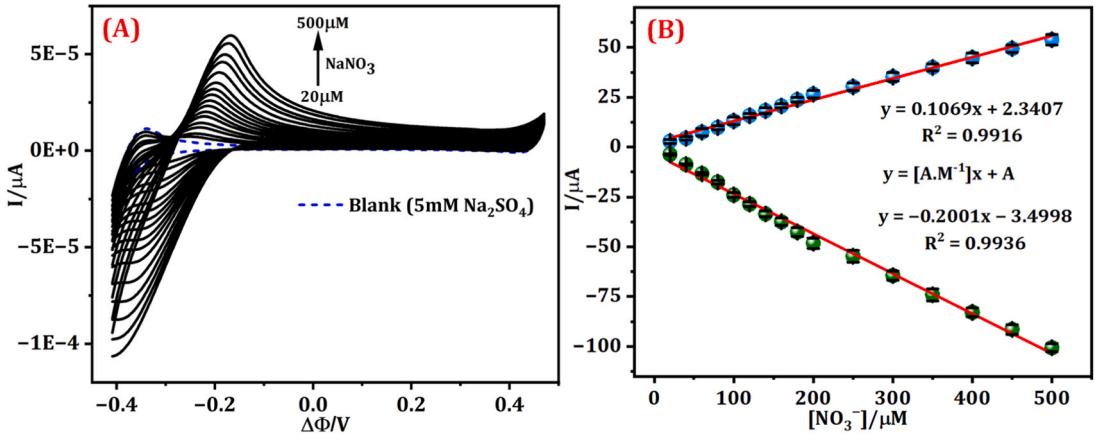

Fig. 3. (A) CVs recorded in Cell-III in the absence and presence of increasing concentration of $NaNO_3$ from 20 to 500 μM, (B) Respective calibration curves plotted based on the analysis of the positive and negative peak current intensities (from part A). The scan rate was 20 $mV.s^{-1}$.

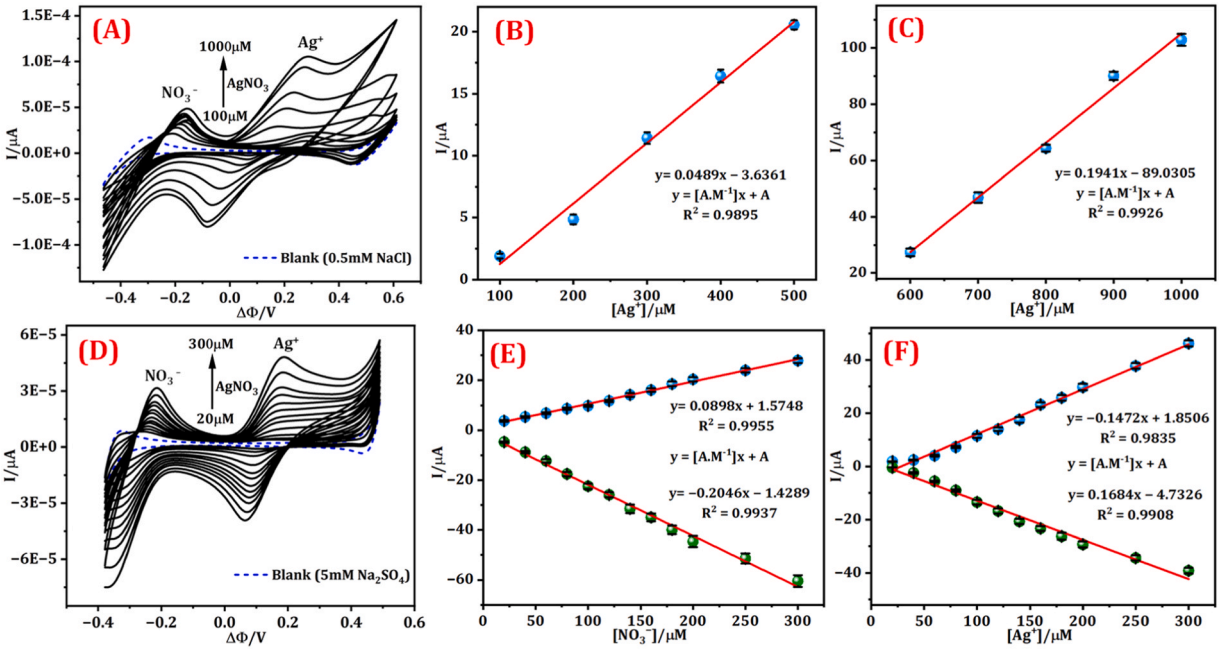

Fig. 4. (A) CVs recorded in Cell-IV in the absence and presence of increasing concentration of $AgNO_3$ from 100 to 1000 μM, (B & C) Linear relationship between the positive current response originating from Ag^+ ion transfer and increasing concentration $AgNO_3$ from 100 to 500 μM (B) and 600–1000 μM. (D) CVs response recorded in Cell-V in absence and presence of increasing concentration of $AgNO_3$ from 20 to 300 μM, (E & F) Linear relationship between the current response related to interfacial transfer of NO_3^- (E) and Ag^+ (F) plotted in function of $AgNO_3$. For CVs the applied scan rate was 20 $mV.s^{-1}$.

species. The CVs of Cell-V composed of 5 mM Na_2SO_4 aqueous phase without and with increasing concentration of $AgNO_3$ (from 20 to 300 μM) were recorded and displayed as Fig. 4D. The CVs show two distinct pair of peaks corresponding to the transfer of nitrate and silver ions from organic to aqueous phase and vice versa. In the given case, it can be noticed that the ion transfer currents of nitrate and silver ion transfer reactions across the interface are found to be linear across the studied concentration range as portrayed by the calibration plots (see Figs. 4E, and 4 F). These findings show that the influence of chloride anions towards nitrate detection at eLLI can be mitigated through the introduction of Ag^+ ions enabling in situ precipitation. This methodology does not involve the introduction of additional chemical species,

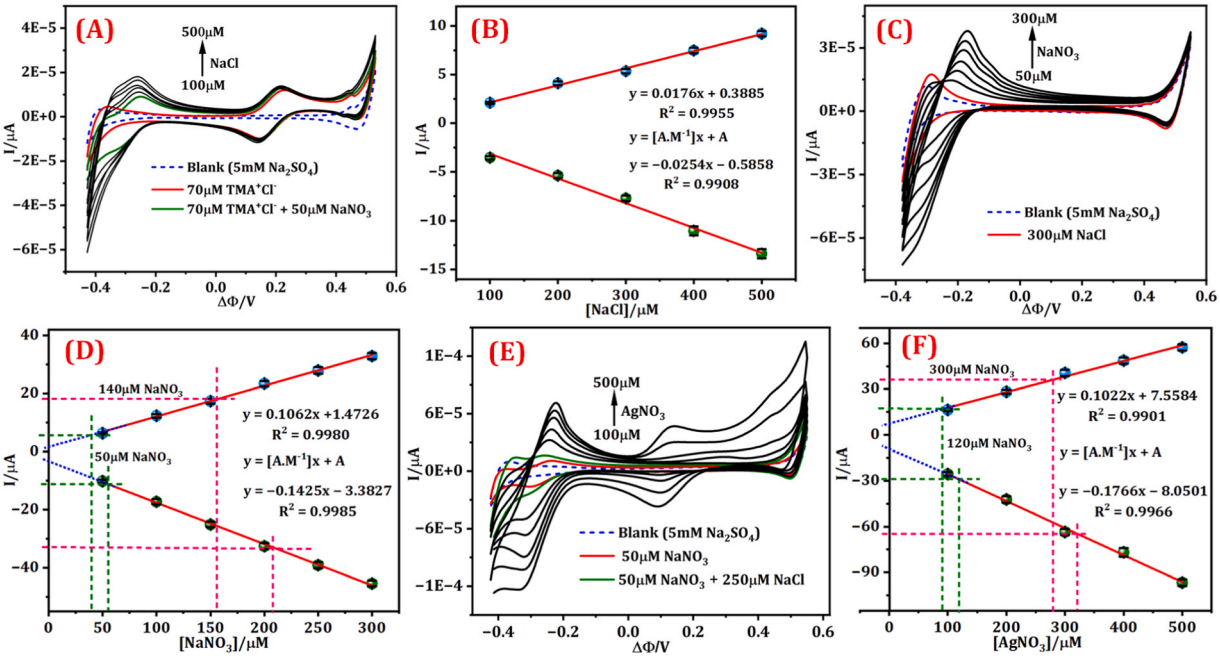

Fig. 5. (A) CV response of Cell-III in the absence and presence of 70 μM TMA^+Cl^-, 70 μM TMA^+Cl^- + 50 μM $NaNO_3$ with increasing concentration of NaCl from 100 to 500 μM, (B) Linear plot of NO_3^- response current plotted in function NaCl concentrations, (C) CV recorded for the increasing concentration of $NaNO_3$ in the absence and in presence of 300 μM NaCl recorded in Cell-III, (D) Linear dependency plotted between the NO_3^- current response plotted in the function of $NaNO_3$ concentration and based on CVs from part (C), (E) CV recorded for the increasing concentration of $AgNO_3$ in the presence of 50 μM of $NaNO_3$, and 50 μM of $NaNO_3$ + 250 μM of NaCl recorded in Cell-III, (F) Corresponding linear dependency plotted between the current response attributed to NO_3^- ion transfer and $AgNO_3$ concentration.

and since $AgNO_3$ is among a few water-soluble inorganic salts it can be applied to build standard addition calibrations curves.

3.4. Understanding and neutralizing the chloride interference

Further, setting the limitations and understanding the effect of potential mitigations to eliminate chloride influence towards the detection of nitrate at eLLI is studied in detail with CV (Fig. 5). At first, CVs were recorded in Cell-III in the presence of model ion (TMACl) and 50 μM $NaNO_3$. The introduction of 50 μM nitrate yields its characteristic ion transfer peak at −0.25 V with a response current of around 9.1 μA for the ion transfer related to NO_3^- heading towards the aqueous phase. Next, the system was titrated against the increasing concentrations of NaCl from 100 μM to 500 μM and the corresponding CVs were recorded (see Fig. 5 A).

The plot of NO_3^- response currents (both positive and negative) against the concentration of NaCl displays a linear relationship with an observed sensitivity of 0.018 $A.M^{-1}$ (for positive peak currents, see Fig. 5B). The CVs and the calibration plots signify that the response current of 500 μM chloride ions is equal to the response currents of 50 μM nitrate ions (10-fold lower concentration). This outcome is further fortified by the observed sensitivity of chloride ion transfer (0.017 $A.M^{-1}$) which is ten times lower than that of the nitrate transfer (0.106 $A.M^{-1}$) observed earlier (Fig. 3B). The average amount of chloride found in freshwater bodies in Poland was reported to be 0.2 ~ 0.3 mM [51,52]. Therefore, the real-time influence of chloride interference is testified by increasing the concentration of nitrate ions in the presence of chloride ions in the aqueous phase side of the eLLI. The CVs recorded in Cell-III in the presence of 0.3 mM NaCl with increasing concentration of nitrate ions are recorded and presented as Fig. 5 C. The voltammograms display characteristic ion transfer peaks attributed to Cl^- at −0.28 V and with the introduction of nitrate the ion transfer peaks shifted to −0.21 V with a sequential rise in response currents upon increasing concentration of nitrate. A plot of the current response against the concentration of nitrate was derived and presented as Fig. 5D. The linear interpolation calculations of nitrate concentrations in the presence of chloride presented only ~5 % deviation at lower concentrations while the deviation elevated significantly to ~20 % for higher concentrations of nitrates in reference to Fig. 3B. This observation implies that the chloride ions possess significant threat towards nitrate detections at higher nitrate concentrations and has to be resolved and improved. Hence, the *in-situ* chemical precipitation studied earlier (Fig. 4D), was adopted to improve the analytical resolution of the eLLI sensing solution and delivered promising outputs (Figs. 5E, 5 F). For this, the CVs recorded in Cell-III in the presence of 50 μM $NaNO_3$ and 250 μM NaCl with increasing concentration (100 – 500 μM) of $AgNO_3$ were recorded and are presented as Fig. 5E. A linear interpolation studies on the calibration plot of NO_3^- response currents plotted against $AgNO_3$ concentration presents improved read out resolutions as the observed signal deviations are dropped to <5 % across the concentration range in reference to Fig. 3B. These findings denote that the *in-situ* chemical precipitation of chloride ions at eLLI is an effective strategy to conceal chloride ion interference towards nitrate detection.

3.5. Interfacial properties of algae nutrient solution at eLLIs

The practical usability of an analytical solution relies on its ability to selectively detect target species in a pool of interfering species in a real-world system. In this respect, we have examined the CV profile of each inorganic nutrient that fuels algal blooms. This was studied in the configuration shown in Cell-VI. The ion transfer voltammograms recorded for all chemical constituents (individually) from the algae grow media are presented in Fig. S1. Numerous studies has confirm that nitrogen in the form of nitrate is a common pollutant in aquatic environment and stimulate rapid cyanobacteria replication leading to harmful algal blooms[53,54]. To emulate this phenomena under laboratory settings a variety of standard culture media for cyanobacteria are proposed including the Z8 medium. The specific recipe of Z8 medium was described by Kotai in 1972 [55]. The Z8 medium is rich in nitrate, phosphate, chloride, and other micro nutrients to catalase the algae growth under controlled environment and chosen for our demonstration of the phenomenon. The Z8 algae nutrient medium is composed of four nutrient solutions (A-D) made up of specific quantities of all the micro and macronutrients. The detailed composition table of the Z8 medium (made of solutions A-D) is presented in Table S2. The CVs recorded in Cell-VI in the absence and for the increasing concentrations of nutrient solutions A-D and its mixture (Z8 medium) were recorded and used to create a calibration plots of current responses (NO_3^- ion transfer) against the concentrations of Z8 medium as presented in Fig. 6. The nutrient solutions A and C are composed of primarily nitrate (solution A), chloride, and carbonate (solution C) displayed its characteristic ion transfer peaks with sequential raise in response current with the increasing concentration of nutrient solutions (Fig. 6 A, and C). Likewise, the nutrient solutions B and D are primarily composed of phosphate (solution B), and micronutrients with trace amounts of nitrates (in solution D) presented their characteristics voltammetric profiles with relatively low response currents than that of solutions A and C (Fig. 6B, and D). At last, the CVs titration of Z8 nutrient medium at the given settings displays a voltammetric profile identical to that of nitrate solutions studied earlier (in Section 3.2). This close signal proximity of Z8 medium can be attributed to the presence of large quantities of nitrate (5.75 mM) followed with significant quantities of phosphate (0.18 mM) mixed with trace extents of other inorganic micronutrients. The calibration plot of Z8 nutrient medium normalized into nitrate concentrations (Fig. 6 F) can be used for the future determination of nitrate concentrations at eLLI in such nutrient rich environments.

3.6. Periodic determination of nitrate levels in algae growth medium at eLLI

The principal objective of this work was to develop an alternative electroanalytical solution for the periodic monitoring of the nitrate plant nutrients that stimulate harmful algal blooms. Prior to on-site adoption, the practicality of the developed eLLI nitrate sensor was testified under *in-vitro* settings with *Microcystis aeruginosa* LEGE 91094 cyanobacteria cultures cultivated in Z8 medium. *Microcystis* is one of the most common species responsible for harmful cyanobacterial blooms worldwide. The occurrence of these organisms in surface water poses a serious risk to human and animal health due to its ability to produce cyanotoxins[56, 57]. The growth of *Microcystis* is directly affected by the nitrogen (in the form of nitrates) and phosphorus (as phosphates) levels in the aquatic system[58–60]. Under laboratory settings, the growth of *M. aeruginosa* will lead to a drop in nitrate concentrations in the nutrient medium. On top of that, monitoring a nitrate concentration (along with other growth medium chemical constituents) would be beneficial for maintaining a healthy and rapidly growing colony. Therefore, during this experiment, the nitrate content in the Z8 medium containing cyanobacteria cultures, considered as a real sample, was tested at eLLI. On this objective, the voltammetric profiles of Z8 medium and its components are recorded earlier (Fig. 6E, and F) and are utilized now to study the periodic determination of nitrate concentrations in *in vitro* cyanobacteria growth samples. First, we calculated the recovery value based on the output of the voltammetric study and the calculated concentration of nitrate at day 0 (this was 161 μM – see Table S2 for the growth medium composition). We have found that the recovery is equal to 97 % which is a very good result for a electroanalytical system. The periodic monitoring experiments are programmed to be performed in the intervals of 7 days starting from day zero to day 14 and the analytical data are presented in Fig. 7. To start, the optical micrographic images of the *Microcystis aeruginosa* LEGE 91094 cyanobacteria cultures captured on day 0, day 7, and day 14 are presented in Fig. 7A. The algae cell densities presented on the respective days were calculated to be 5.13×10^{-3}, 1.59×10^{-5}, and

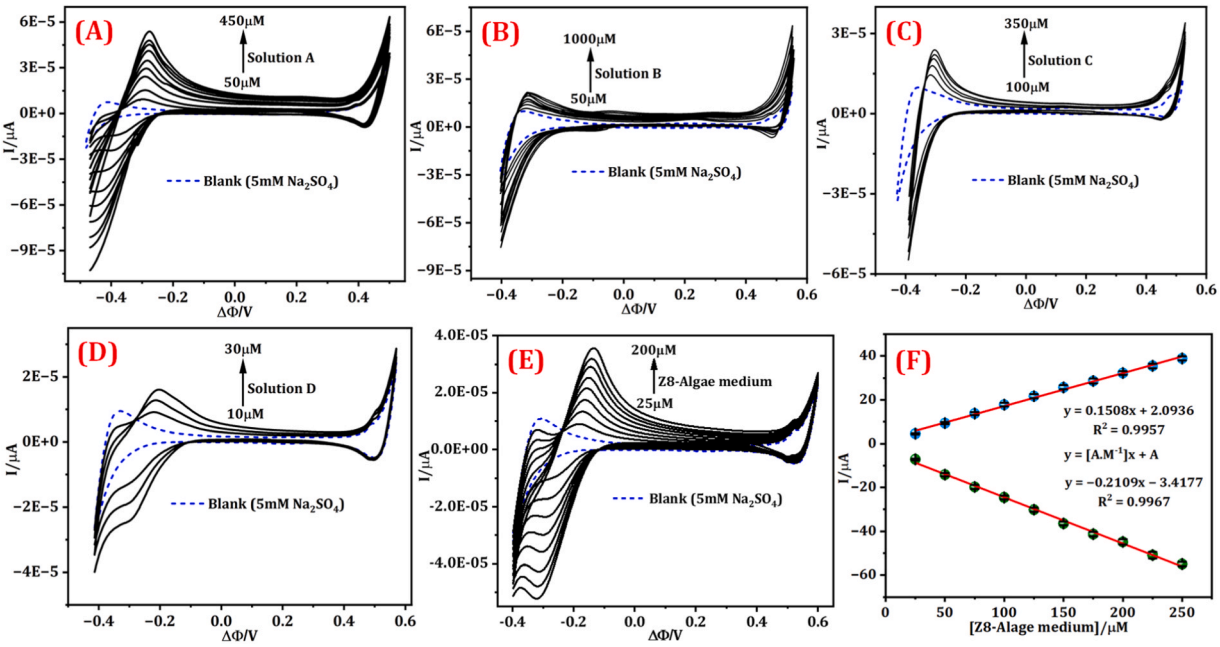

Fig. 6. (A-E) CVs of increasing concentrations of algae nutrients solutions and its mixture; (A) solution A, (B) solution B, (C) solution C, (D) solution D, (E) Z8-medium, (F) Linear plot between the current response of Z8-medium and its different concentrations.

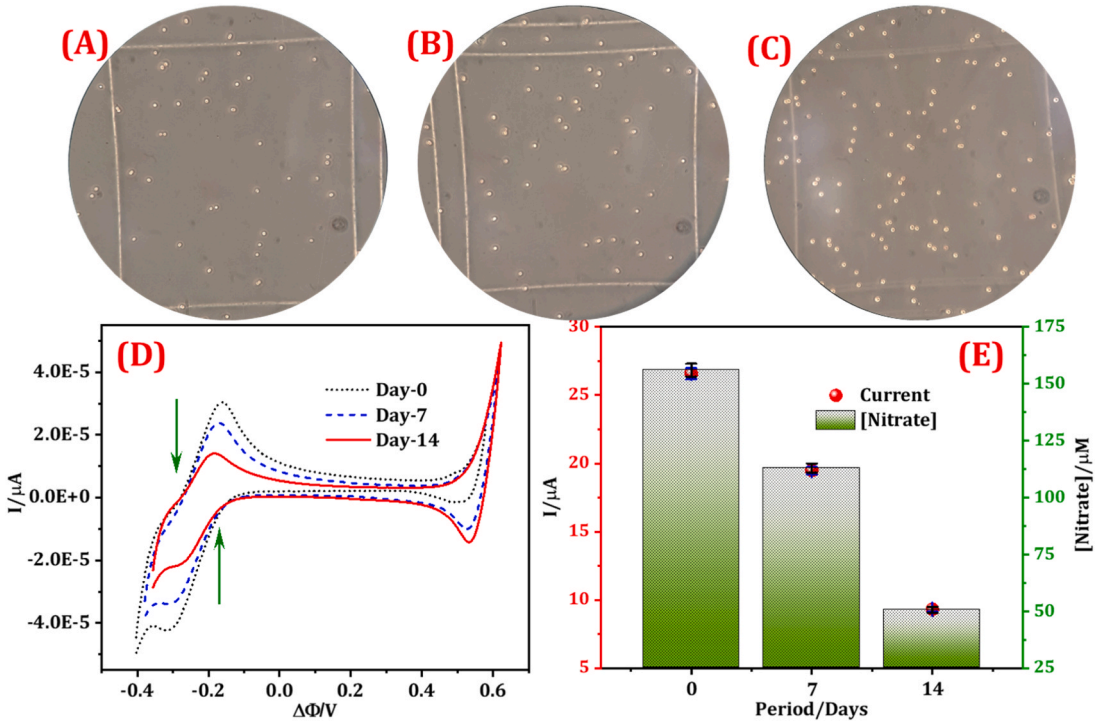

Fig. 7. Optical micrographic images of *Microcystis aeruginosa* LEGE 91094 cyanobacteria in Z8 medium from day 0 (A, no dilution) day 7 (B, diluted 2-times), day 14 (C, diluted 3-times), (D) Ion transfer voltammograms of *Microcystis aeruginosa* LEGE 91094 cyanobacteria in Z8 medium (93 µL) recorded on day zero, day 7, and day 14, (E) A bar chart translating response current into concentration of nitrate from day zero to day 14.

3.64×10^{-5} cells.mL^{-1}, correspondingly. The CV titrations of *Microcystis aeruginosa* LEGE 91094 cyanobacteria samples (with and without centrifugation) recorded in Cell-VI were recorded on day 0, day 7, and day 14 and its calibration plots of response currents against the volume of algae samples (15.5 – 93 µL) are presented and discussed in detail in the Supporting information (Fig. S2 and S3). A simple overlay of CV profiles of *Microcystis aeruginosa* LEGE 91094 cyanobacteria solutions – cultures (93 µL, uncentrifuged) recorded on day 0, day 7, and day 14 is presented as Fig. 7D. The CV curves dissipate a sequential drop in response currents related to nitrate ion transfer (i.e. drop in nitrate concentrations) upon algae growth from day 0 to day 14. This extensive drop in response currents corresponding to nitrate ion transfer denotes vast consumption of nitrate by *Microcystis aeruginosa* LEGE 91094 cyanobacteria cultures upon its growth as observed in the micrographs of

days 0–14 in Fig. 7A-C. Further, a plot of response currents normalized into nitrate concentration was also derived and projected as Fig. 7E. This plot highlights the relationship between the response currents of nitrate ion transfer and the concentration of nitrate in algae solutions with respect to cyanobacterial growth. These findings emphasize that the developed eLLI-based nitrate sensing platform is successful in the on-site periodic monitoring of nitrate ions in the cyanobacteria growth samples with good consistency and analytical reliability without any pretreatment. We are currently extending the proposed methodology towards phosphate detection along with the products of algae metabolism. All this information is expected to provide electroanalytical tools that can be used for cyanobacteria blooms predictions and monitoring. The developed eLLI platform is quite successful in the quantitative assessment of nitrate levels in cyanobacteria growth nutrient medium under a controlled environment under a poll of other inorganic ions. However, the real-world algal bloom samples could be rich in other aquatic pollutants including heavy metals, pigments, and other organic matters [61–63] that are not tested as a part of our study. Thus, these species may influence the analytical results during real-world implementation of the system, and are a potential topic for further investigation that falls beyond the scope of the present work.

4. Conclusion

In this work, we present an alternative electroanalytical platform for rapid on-site detection and periodic monitoring of nitrate plant nutrients present in in-vitro algae growth solutions through a simple cyclic voltammetry technique. The interfacial transfer of nitrate ions across the interface formed between the aqueous and 1,2-dichloroethane solution was studied and optimized to minimize the influence of chloride ions toward the detection of nitrate. A simple *in situ* chemical precipitation strategy using $AgNO_3$ precipitant was developed to eliminate the influence of chloride ions in the analytical detection of nitrate at eLLI. The key analytical parameters such as linear dynamic range, the limit of detection, and quantification of the eLLI-based nitrate sensors were extracted to be 20–500 μM, 1.5 μM, and 14.6 μM, respectively. Up next, the cyclic voltammetry profiles of other common inorganic plant nutrients that constitute Z8 nutrient medium are recorded to scrutinize the influence of these co-existing species in the analytical detection of nitrate in algae growth samples. Before studies focused on cyanobacteria growth medium, the analytical signal of nitrate sensing in eLLI was extensively studied in Z8 cyanobacteria medium, and corresponding calibration plots were established. The practicality of the developed eLLI-nitrate sensor was demonstrated with in-vitro periodic monitoring of nitrate concentrations in *Microcystis aeruginosa* LEGE 91094 cyanobacteria cultures (in Z8 medium) up to 14 days with an interval of 7 days. The analytical observations are in full compliance with the micrographic observations of cyanobacteria growth and its consequent drop in nitrate concentrations highlights the practical feasibility of the eLLI-based nitrate sensing solution.

CRediT authorship contribution statement

Thangaraj Balamurugan: Writing – review & editing, Formal analysis. **Karolina Czarny-Krzymińska:** Writing – review & editing, Resources, Formal analysis. **Karolina Marciniak:** Writing – review & editing, Formal analysis, Data curation. **Lukasz Poltorak:** Writing – review & editing, Supervision, Methodology, Funding acquisition, Conceptualization. **Muthaiah Annalakshmi:** Writing – original draft, Validation, Investigation, Funding acquisition, Formal analysis, Data curation, Conceptualization.

Declaration of Competing Interest

The authors declare the following financial interests/personal relationships which may be considered as potential competing interests: Muthaiah Annalakshmi reports financial support was provided by National Science Centre Poland. If there are other authors, they declare that they have no known competing financial interests or personal relationships that could have appeared to influence the work reported in this paper.

Acknowledgements

M.A. and L.P. gratefully acknowledge the financial assistance through the PolonezBis fellowship (Project No. 2022/47/P/ST4/01065) co-funded by the National Science Centre (NCN) - experiments at the electrifed liquid-liquid interface, algae cultivation. T.S.T.B is grateful to the European Union's Horizon Europe Horizon-WIDERA program grant agreement No. 101090335 for his ERA fellowship.

Data statement

Data published in this work are uploaded to the data repository: DOI: 10.5281/zenodo.13958275.

Appendix A. Supporting information

Supplementary data associated with this article can be found in the online version at doi:10.1016/j.snb.2024.136863.

Data Availability

Data will be made available on request or are available through scientific repository: DOI 10.5281/zenodo.13958274.

References

[1] A. Wany, C.H. Foyer, K.J. Gupta, Nitrate, NO and ROS signaling in stem cell homeostasis, Trends Plant Sci. 23 (2018) 1041–1044, https://doi.org/10.1016/J.TPLANTS.2018.09.010.
[2] Y.Y. Wang, P.K. Hsu, Y.F. Tsay, Uptake, allocation and signaling of nitrate, Trends Plant Sci. 17 (2012) 458–467, https://doi.org/10.1016/J.TPLANTS.2012.04.006.
[3] S.J. Leghari, N.A. Wahocho, G.M. Laghari, A. HafeezLaghari, G. MustafaBhabhan, K. HussainTalpur, T.A. Bhutto, S.A. Wahocho, A.A. Lashari, Role of nitrogen for plant growth and development: a review, Adv. Environ. Biol. 10 (2016) 209–219. ⟨https://go.gale.com/ps/i.do?p=AONE&sw=w&issn=19950756&v=2.1&it=r&id=GALE%7CA472372583&sid=googleScholar&linkaccess=fulltext⟩ (accessed June 19, 2024).
[4] R.M. Keller, L. Beaver, M.C. Prater, N.G. Hord, Dietary nitrate and nitrite concentrations in food patterns and dietary supplements, Nutr. Today 55 (2020) 218–226, https://doi.org/10.1097/NT.0000000000000253.
[5] N.S. Bryan, H. van Grinsven, The role of nitrate in human health, Adv. Agron. 119 (2013) 153–182, https://doi.org/10.1016/B978-0-12-407247-3.00003-2.
[6] Y.J. Shih, Z.L. Wu, Y.H. Huang, C.P. Huang, Electrochemical nitrate reduction as affected by the crystal morphology and facet of copper nanoparticles supported on nickel foam electrodes (Cu/Ni), Chem. Eng. J. 383 (2020) 123157, https://doi.org/10.1016/J.CEJ.2019.123157.
[7] G. Li, H. Yuan, J. Mou, E. Dai, H. Zhang, Z. Li, Y. Zhao, Y. Dai, X. Zhang, Electrochemical detection of nitrate with carbon nanofibers and copper co-modified carbon fiber electrodes, Compos. Commun. 29 (2022) 101043, https://doi.org/10.1016/J.COCO.2021.101043.
[8] M.E.E. Alahi, S.C. Mukhopadhyay, Detection methods of nitrate in water: a review, Sens Actuators A Phys. 280 (2018) 210–221, https://doi.org/10.1016/J.SNA.2018.07.026.
[9] P. Kalimuthu, T. Kruse, P.V. Bernhardt, A highly sensitive and stable electrochemical nitrate biosensor, Electro Acta 386 (2021) 138480, https://doi.org/10.1016/J.ELECTACTA.2021.138480.
[10] X. Jiang, G. Gao, L. Zhang, X. Tang, K. Shao, Y. Hu, Denitrification and dissimilatory nitrate reduction to ammonium in freshwater lakes of the Eastern Plain, China: influences of organic carbon and algal bloom, Sci. Total Environ. 710 (2020) 136303, https://doi.org/10.1016/J.SCITOTENV.2019.136303.
[11] D. Rosales, A. Ellett, J. Jacobs, G. Ozbay, S. Parveen, J. Pitula, Investigating the relationship between nitrate, total dissolved nitrogen, and phosphate with abundance of pathogenic vibrios and harmful algal blooms in rehoboth bay, delaware, Appl. Environ. Microbiol 88 (2022), https://doi.org/10.1128/AEM.00356-22/SUPPL_FILE/AEM.00356-22-S0001.PDF.
[12] S.G. Woo, S.J. Moon, S.K. Kim, T.H. Kim, H.S. Lim, G.H. Yeon, B.H. Sung, C.H. Lee, S.G. Lee, J.H. Hwang, D.H. Lee, A designed whole-cell biosensor for live diagnosis of gut inflammation through nitrate sensing, Biosens. Bioelectron. 168 (2020) 112523, https://doi.org/10.1016/J.BIOS.2020.112523.

[13] B. Patella, R.R. Russo, A. O'Riordan, G. Aiello, C. Sunseri, R. Inguanta, Copper nanowire array as highly selective electrochemical sensor of nitrate ions in water, Talanta 221 (2021) 121643, https://doi.org/10.1016/J.TALANTA.2020.121643.
[14] M.H. Ward, R.R. Jones, J.D. Brender, T.M. de Kok, P.J. Weyer, B.T. Nolan, C. M. Villanueva, S.G. van Breda, Drinking water nitrate and human health: an updated review, Page 1557, Int. J. Environ. Res. Public Health 2018, Vol. 15 15 (2018) 1557, https://doi.org/10.3390/IJERPH15071557.
[15] R.K.A. Amali, H.N. Lim, I. Ibrahim, N.M. Huang, Z. Zainal, S.A.A. Ahmad, Significance of nanomaterials in electrochemical sensors for nitrate detection: a review, Trends Environ. Anal. Chem. 31 (2021) e00135, https://doi.org/10.1016/J.TEAC.2021.E00135.
[16] K.S. Johnson, L.J. Coletti, H.W. Jannasch, C.M. Sakamoto, D.D. Swift, S.C. Riser, Long-term nitrate measurements in the ocean using the in situ ultraviolet spectrophotometer: sensor integration into the APEX profiling float, J. Atmos. Ocean Technol. 30 (2013) 1854–1866, https://doi.org/10.1175/JTECH-D-12-00221.1.
[17] M. Sepahvand, F. Ghasemi, H.M. Seyed Hosseini, Plasmonic nanoparticles for colorimetric detection of nitrite and nitrate, Food Chem. Toxicol. 149 (2021) 112025, https://doi.org/10.1016/J.FCT.2021.112025.
[18] M.F. Khanfar, W. Al-Faqheri, A. Al-Halhouli, Low cost lab on chip for the colorimetric detection of nitrate in mineral water products, Sens. 2017, Vol. 17, Page 2345 17 (2017) 2345, https://doi.org/10.3390/S17102345.
[19] M. Akyüz, Ata, Determination of low level nitrite and nitrate in biological, food and environmental samples by gas chromatography–mass spectrometry and liquid chromatography with fluorescence detection, Talanta 79 (2009) 900–904, https://doi.org/10.1016/J.TALANTA.2009.05.016.
[20] E. Murray, P. Roche, M. Briet, B. Moore, A. Morrin, D. Diamond, B. Paull, Fully automated, low-cost ion chromatography system for in-situ analysis of nitrite and nitrate in natural waters, Talanta 216 (2020) 120955, https://doi.org/10.1016/J.TALANTA.2020.120955.
[21] E. Martínková, T. Křžek, P. Coufal, Determination of nitrites and nitrates in drinking water using capillary electrophoresis, Chem. Pap. 68 (2014) 1008–1014, https://doi.org/10.2478/S11696-014-0548-4/METRICS.
[22] J.E. Melanson, C.A. Lucy, Ultra-rapid analysis of nitrate and nitrite by capillary electrophoresis, J. Chromatogr. A 884 (2000) 311–316, https://doi.org/10.1016/S0021-9673(99)01340-0.
[23] M. Joly, M. Marlet, C. Durieu, C. Bene, J. Launay, P. Temple-Boyer, Study of chemical field effect transistors for the detection of ammonium and nitrate ions in liquid and soil phases, Sens Actuators B Chem. 351 (2022) 130949, https://doi.org/10.1016/J.SNB.2021.130949.
[24] X. Chen, H. Pu, Z. Fu, X. Sui, J. Chang, J. Chen, S. Mao, Real-time and selective detection of nitrates in water using graphene-based field-effect transistor sensors, Environ. Sci. Nano 5 (2018) 1990–1999, https://doi.org/10.1039/C8EN00588E.
[25] M. Darestani-Farahani, F. Ma, V. Patel, P.R. Selvaganapathy, P. Kruse, An ion-selective chemiresistive platform as demonstrated for the detection of nitrogen species in water, Analyst 148 (2023) 5731–5744, https://doi.org/10.1039/D3AN01267K.
[26] L. Li, P. Du, Y. Zhang, Y. Duan, Y. Li, Y. Qian, P. Zhang, Q. Guo, Deploying hydrogen bond donor/acceptor on arylethynyl scaffold II: Urea based tripodal ionophores for polymeric membrane nitrate selective electrodes, Sens Actuators B Chem. 329 (2021) 129151, https://doi.org/10.1016/J.SNB.2020.129151.
[27] P. Damala, E. Zdrachek, E. Bakker, Commercially available nitrate ionophores in potentiometric sensors are not superior to common ion-exchangers, Electroanalysis 35 (2023) e202200247, https://doi.org/10.1002/ELAN.202200247.
[28] N.P. Revsbech, M. Nielsen, D. Fapyane, Ion selective amperometric biosensors for environmental analysis of nitrate, nitrite and sulfate, Sens. 2020, Vol. 20, Page 4326 20 (2020) 4326, https://doi.org/10.3390/S20154326.
[29] S. Sudalaimani, K. Sanjeev Kumar, A. Esokkiya, C. Suresh, K. Giribabu, Electrified liquid–liquid interface as an electrochemical tool for the sensing of putrescine and cadaverine, Analyst 146 (2021) 3208–3215, https://doi.org/10.1039/D1AN00019E.
[30] N.T. Iwai, M. Kramaric, D. Crabbe, Y. Wei, R. Chen, M. Shen, GABA detection with nano-ITIES Pipet electrode: a new mechanism, water/DCE-octanoic acid interface, Anal. Chem. 90 (2018) 3067–3072, https://doi.org/10.1021/ACS.ANALCHEM.7B03099.
[31] R. Chen, A.B. McAllister, M. Shen, Detection of zwitterion at an electrified liquid-liquid interface: a chemical equilibrium perspective, J. Electroanal. Chem. 873 (2020) 114303, https://doi.org/10.1016/J.JELECHEM.2020.114303.
[32] D.W.M. Arrigan, M.J. Hackett, R.L. Mancera, Electrochemistry of proteins at the interface between two immiscible electrolyte solutions, Curr. Opin. Electrochem 12 (2018) 27–32, https://doi.org/10.1016/J.COELEC.2018.07.012.
[33] K. Rudnicki, K. Sobczak, P. Borgul, S. Skrzypek, L. Poltorak, Determination of quinine in tonic water at the miniaturized and polarized liquid–liquid interface, Food Chem. 364 (2021) 130417, https://doi.org/10.1016/j.foodchem.2021.130417.
[34] K. Rudnicki, L. Poltorak, S. Skrzypek, E.J.R. Sudholter, Ion transfer voltammetry for analytical screening of fluoroquinolone antibiotics at the water – 1.2-dichloroethane interface, Anal. Chim. Acta 1085 (2019) 75–84, https://doi.org/10.1016/j.aca.2019.07.065.
[35] T.S.T. Balamurugan, P. Stelmaszczyk, R. Wietecha-Posluszny, L. Poltorak, Electroanalytical characterization of clozapine at the electrified liquid-liquid interface and its detection in soft and hard drinks, Analyst (2024), https://doi.org/10.1039/D3AN02188B.
[36] P. Borgul, K. Sobczak, K. Rudnicki, A. Leniart, S. Skrzypek, L. Poltorak, Oxidized thin aluminum films used as the polarized liquid-liquid interface support for norcocaine detection, Sens Actuators B Chem. 373 (2022) 132651, https://doi.org/10.1016/j.snb.2022.132651.
[37] L. Poltorak, I. Eggink, M. Hoitink, E.J.R. Sudhölter, M. de Puit, Electrified soft interface as a selective sensor for cocaine detection in street samples, Anal. Chem. 90 (2018) 7428–7433, https://doi.org/10.1021/acs.analchem.8b00916.
[38] H.H.J. Girault, D.J. Schiffrin, Electrochemistry of liquid-liquid interfaces, Electroanal. Chem.: A Ser. Adv.: Vol. 15 15 (2023) 1–141, https://doi.org/10.1201/9781003418115-1/ELECTROCHEMISTRY-LIQUID-LIQUID-INTERFACES-GIRAULT-SCHIFFRIN.
[39] X. Zhao, X. Lu, Q. Zheng, L. Fang, L. Zheng, X. Chen, Z.L. Wang, Studying of contact electrification and electron transfer at liquid-liquid interface, Nano Energy 87 (2021) 106191, https://doi.org/10.1016/J.NANOEN.2021.106191.
[40] T.J. Stockmann, J. Zhang, J.C. Wren, Z. Ding, Hydrophobic alkylphosphonium ionic liquid for electrochemistry at ultramicroelectrodes and micro liquid|liquid interfaces, Electro Acta 62 (2012) 8–18, https://doi.org/10.1016/J.ELECTACTA.2011.10.087.
[41] Q. Qian, G.S. Wilson, K. Bowman-James, H.H. Girault, MicroITIES Detection of Nitrate by Facilitated Ion Transfer, Anal. Chem. 73 (2000) 497–503, https://doi.org/10.1021/AC000806H.
[42] D. Hu, H. Wang, K. Gao, X. Jiang, M. Wang, Y. Long, Y. Chen, Anion transfer across "anion channels" at the liquid/liquid interface modified by anion-exchange membrane, RSC Adv. 4 (2014) 57035–57040, https://doi.org/10.1039/c4ra09985k.
[43] S. Nisha Nandhini, N. Stalin, Isolation of toxin producing cyanobacteria from aquatic samples: oscillatoria, Protoc. Cyanobacteria Sampl. Detect. Cyanotoxin (2023) 123–126, https://doi.org/10.1007/978-981-99-4514-6_17.
[44] J. Kotai, Instructions for preparation of modified nutrient solution Z8 for algae, Oikos 15 (1972) 155–164.
[45] K. Sobczak, K. Rudnicki, L. Jedinak, M. Zatloukalova, J. Vacek, L. Poltorak, Oleic and nitro-oleic acid behavior at an electrified water-1,2-dichloroethane interface, J. Mol. Liq. 365 (2022) 120110, https://doi.org/10.1016/j.molliq.2022.120110.
[46] B. Schazmann, D. Diamond, Improved nitrate sensing using ion selective electrodes based on urea – calixarene ionophores, New J. of Chemistry 31 (2007) 587–592, https://doi.org/10.1039/B702841P.
[47] G.A. Crespo, Recent Advances in Ion-selective membrane electrodes for in situ environmental water analysis, Electro Acta 245 (2017) 1023–1034, https://doi.org/10.1016/J.ELECTACTA.2017.05.159.
[48] H.D.B. Jenkins, K.P. Thakur, Reappraisal of Thermochemical Radii for Complex Ions, J. Chem. Educ. 56 (1979) 576–577. ⟨https://pubs.acs.org/doi/pdf/10.1021/ed056p576⟩ (accessed May 24, 2024).
[49] Y. Li, Z. Yang, K. Yang, J. Wei, Z. Li, C. Ma, X. Yang, T. Wang, G. Zeng, G. Yu, Z. Yu, C. Zhang, Removal of chloride from water and wastewater: Removal mechanisms and recent trends, Sci. Total Environ. 821 (2022) 153174, https://doi.org/10.1016/J.SCITOTENV.2022.153174.
[50] L.P. Wang, W.H. Lee, S.M. Tseng, T.W. Cheng, Removal of chloride ions from an aqueous solution containing a high chloride concentration through the chemical precipitation of friedel's salt, Mater. Trans. 59 (2018) 297–302, https://doi.org/10.2320/MATERTRANS.M2017273.
[51] B. Kończak, E. Janson, Risk analysis for groundwater intake in an old mining shaft with increased chloride content, Upper Silesia, Southern Poland, J. Water Health 19 (2021) 288–305, https://doi.org/10.2166/WH.2021.144.
[52] H.A. Dugan, J.C. Summers, N.K. Skaff, F.E. Krivak-Tetley, J.P. Doubek, S.M. Burke, S.L. Bartlett, L. Arvola, H. Jarjanazi, J. Korponai, A. Kleeberg, G. Monet, D. Monteith, K. Moore, M. Rogora, P.C. Hanson, K.C. Weathers, Long-term chloride concentrations in North American and European freshwater lakes, Sci. Data 2017 4 1 4 (2017) 1–11, https://doi.org/10.1038/sdata.2017.101.
[53] E.Craswell Bijay-Singh, Fertilizers and nitrate pollution of surface and ground water: an increasingly pervasive global problem, SN Appl. Sci. 2021 3 4 3 (2021) 1–24, https://doi.org/10.1007/S42452-021-04521-8.
[54] C. Vézie, J. Rapala, J. Vaitomaa, J. Seitsonen, K. Sivonen, Effect of nitrogen and phosphorus on growth of toxic and nontoxic microcystis strains and on intracellular microcystin concentrations, Micro Ecol. 43 (2002) 443–454. ⟨http://www.jstor.org/stable/4287619⟩.
[55] J. Kotai, Instruction of preparations of modified nutrient medium Z8 for algae, Norw. Inst. Water Res. Blind. Oslo (1972) 32–39.
[56] S. Merel, D. Walker, R. Chicana, S. Snyder, E. Baurès, O. Thomas, State of knowledge and concerns on cyanobacterial blooms and cyanotoxins, Environ. Int 59 (2013) 303–327, https://doi.org/10.1016/J.ENVINT.2013.06.013.
[57] R.P. Rastogi, R.P. Sinha, A. Incharoensakdi, The cyanotoxin-microcystins: current overview, Rev. Environ. Sci. Biotechnol. 13 (2014) 215–249, https://doi.org/10.1007/S11157-014-9334-6/TABLES/2.
[58] P. Geada, R.N. Pereira, V. Vasconcelos, A.A. Vicente, B.D. Fernandes, Assessment of synergistic interactions between environmental factors on Microcystis aeruginosa growth and microcystin production, Algal Res 27 (2017) 235–243, https://doi.org/10.1016/J.ALGAL.2017.09.006.
[59] B. George, I. Pancha, C. Desai, K. Chokshi, C. Paliwal, T. Ghosh, S. Mishra, Effects of different media composition, light intensity and photoperiod on morphology and physiology of freshwater microalgae ankistrodesmus falcatus – a potential strain for bio-fuel production, Bioresour. Technol. 171 (2014) 367–374, https://doi.org/10.1016/J.BIORTECH.2014.08.086.
[60] K. Sangapillai, T. Marimuthu, Isolation and selection of growth medium for freshwater microalgae Asterarcys quadricellulare for maximum biomass production, Water Sci. Technol. 80 (2019) 2027–2036, https://doi.org/10.2166/WST.2020.015.

[61] A. Ojha, D. Tiwary, Organic pollutants in water and its health risk assessment through consumption, Contam. Water.: Health Risk Assess. Treat. Strateg. (2021) 237–250, https://doi.org/10.1016/B978-0-12-824058-8.00039-6.
[62] X. You, N. Xu, X. Yang, W. Sun, Pollutants affect algae-bacteria interactions: a critical review, Environ. Pollut. 276 (2021) 116723, https://doi.org/10.1016/J.ENVPOL.2021.116723.
[63] B.E. Lapointe, L.W. Herren, A.L. Paule, Septic systems contribute to nutrient pollution and harmful algal blooms in the St. Lucie Estuary, Southeast Florida, USA, Harmful Algae 70 (2017) 1–22, https://doi.org/10.1016/J.HAL.2017.09.005.

Muthaiah Annalakshmi is a MSCA PolonezBis fellow in the Electrochemistry at soft interface team at the Faculty of Chemistry, University of Lodz, Poland. Her research theme is about engineering tailored nanomaterials, corrosion resistant high entropy alloy coatings, and thin polymeric membranes for electrochemical sensing and biosensing, energy storage, and conversion applications. Now she is focusing on developing simple, cost-effective materials and fabrication tools for real-time monitoring and quantification of various analytical targets ranging from environmental pollutants, toxins, drugs, and biomolecules with minimal to no preprocessing of real world samples of aquatic, food, pharmaceutical, and live cell medium.

Thangaraj S T Balamurugan is a MSCA-WIDERA postdoctoral fellow in the Electrochemistry at soft interface team at the Faculty of Chemistry, University of Lodz, Poland. His research span across the fields of analytical, organic, and material chemistry. He aims at developing alternative analytical platforms for biomedical and forensic analysis through low cost fabrication and molecular design principles. His intersts and expertise includes developing stimuli responsive electrochemcial and colorimetric sensors. enginering designer materials for (bio)sensing, energy harwesing, self-powered devices, werable electrocnics, etc.

Karolina Czarny-Krzymińska received her Ph.D. from the Faculty of Chemistry of University of Lodz (Lodz, Poland) in 2019. Her research area includes analytical chemistry, environmental pollution, environmental protection, water quality and cyanobacterial blooms.

Karolina Sobczak is a 3nd year PhD student working at the Faculty of Chemistry, University of Lodz. She is also a PI of the Preludium project entitled “Polarized gel-gel interfaces supported with a 3D printed cell for the urine diagnosis:. Karolina Sobczak is currently focused on 3D printing-based fabrication for electroanalytical applications.

Lukasz Poltorak received his Ph.D. from Lorraine University (Nancy, France) in Chemistry in 2015. From 2015–2018 he was working as the post-doctoral fellow at Delft University of Technology in Organic Materials & Interfaces Group (The Netherlands). From 2019–2021 he was hired as an assistant professor, and since 2022 as a University professor working at the Faculty of Chemistry, University of Lodz (Poland). Currently, he is a leader of the Electrochemistry@Soft Interfaces (E@SI) team. His main scientific interest covers electrochemistry at soft interfaces, including electrified liquid-liquid interfaces, electrochemistry of membranes, (bio)sensors development, biointerfaces investigation, and electrochemistry of/for soft matter.